The Coupled Effects of Mantle Mixing and a Water-Dependent Viscosity on the Surface Ocean

Kiran Chotalia*[1], Neil Cagney[2], Carolina Lithgow-Bertelloni[3], John Brodholt[1,4]

[1]Department of Earth Sciences, University College London, Gower Street, London, WC1E 6BT, UK

[2]Department of Mechanical Engineering, University College London, Gower Street, London, WC1E 6BT, UK

[3]Department of Earth, Planetary, and Space Sciences, University of California, Los Angeles, 595 Charles Young Drive East, Los Angeles, CA 90095-1567, USA

[4]Centre for Earth Evolution and Dynamics (CEED), University of Oslo, 0316 Oslo, Norway

*Corresponding Author, kiran.chotalia.11@ucl.ac.uk

words: 5399, figures: 9, references: 23

Abstract

Water content plays a vital role in determining mantle rheology and thus mantle convection and plate tectonics. Most parameterised convection models predict that the Earth initially underwent a period of rapid degassing and heating, followed by a slow and sustained period of regassing and cooling. However, these models assume water is instantaneously mixed and homogeneously distributed into the mantle. This is a limitation because the mixing time for water entering and leaving the mantle is a function of the Rayleigh number which varies dramatically with water content, temperature, and through time. Here we present an adapted parametrised model (Crowley et al., 2011) to include the coupled effects of the time scale of mixing with a water-dependent viscosity. We consider two cases: first, where the mixing time is constant throughout the model and second, where mixing time varies as a response to an evolving Rayleigh number. The results are compared to a standard case of instantaneous mixing. We find that, facilitated by the water-dependence of the melting depth, a constant mixing time can have huge effect on water content evolution and, in particular, induces long periods of degassing. The inclusion of a variable mixing time dependent on the Rayleigh number acts to limit the period of degassing and also results in more water being stored in the mantle and less at the surface than in both the constant and instantaneous mixing cases. Small changes in the surface ocean induced by mixing times on the order of 0.1 Gyrs can cause changes in the global-mean sea level on the order of 10's of metres. These changes in sea level could easily uncover topographic highs in the bathymetry, potentially aiding subaerial erosion and continental crust, processes thought to be important. Even in this relatively simple model, the inclusion of a mixing time between water entering and leaving the mantle creates a more dynamic water cycle and shows that local heterogeneity in mantle water content can greatly affect the deep water cycle through time. This emphasises the importance of understanding the heterogeneous distribution of water in the Earth's mantle.

Keywords: mixing, water-dependent viscosity, sea level, parametrised mantle convection

1 Introduction

Viscosity depends on many parameters including temperature, pressure and grain size but the effect of water is currently undergoing investigation. Laboratory experiments on olivine have shown that water content can cause a reduction in viscosity of up to three orders of magnitude (e.g. Mei and Kohlstedt, 2000; Fei et al., 2013) and numerical experiments on perovskite show almost no effect (Muir and Brodholt, 2018). Understanding this relationship between mineral viscosity and water content is of particular interest due to the implications for mantle convection and hence planetary evolution. If viscosity can vary several orders of magnitude, the convective vigour could also change by this magnitude with consequences for the style of convection.

The effects of a water-dependent viscosity on thermal evolution have been examined previously in parametrised (Crowley et al., 2011; Sandu et al., 2011) and two-dimensional (2D) models (e.g. Nakagawa et al., 2015). Parametrised studies have shown a water-dependent viscosity initially produces a period of heating and a state of net degassing (where degassing at MORs exceeds regassing at subduction zones), followed by a long and sustained period of cooling and a state of net regassing (Crowley et al., 2011; Sandu et al., 2011). This is due to the rapidly decreasing water content increasing the viscosity, trapping heat and causing the temperature to build up. After some time, the increase in temperature lowers the viscosity and increases Ra such that the mantle starts to convect more efficiently again and the mantle ends up in a period of gradual cooling and regassing. Some models suggest more than one cycle of heating and cooling have occurred over the lifetime of the Earth (Sandu et al., 2011). The initial period of degassing removes almost all of the water from the mantle reservoir resulting in a drier mantle, something that has been suggested to aid the onset of plate tectonics (Korenaga, 2011) and could explain the evidence of slow cooling from petrological data (Seales and Lenardic, 2018). A water-dependent viscosity has also been coupled with continent generation showing that increased continental weathering due to the presence of life on Earth favours a wet mantle (Höning et al., 2014; Höning and Spohn, 2016).

One of the biggest assumptions in parametrised models is that mixing of water introduced at subduction zones and extracted at mid-ocean ridge (MORs) is instantaneous and moreover, the water is homogeneously distributed throughout the mantle. This, of course, is a great simplification.

Consider a subducted package that follows the trajectory shown in Figure 1, travelling a total distance $P = 2d + L$. The time it takes to reach the MOR is then the mixing time $\tau = {}^{P}/_{U}$. τ is also likely to depend on the convective vigour, Ra (where Ra is the ratio of buoyancy to dissipative forces). As the velocity $U \propto Ra^{\frac{2}{3}}$ (Turcotte and Oxburgh, 1967), $\tau \propto Ra^{-\frac{2}{3}}$ and the mixing time is inversely proportional to the convective vigour. This implies that in the past when the mantle was hotter, viscosity was low, Ra was high and the mixing time was short. As it cools the viscosity increases, Ra decreases and τbecomes longer.

It is clear that both water content and mixing time play vital roles in the mantle, and that the two variables are strongly interdependent. However, in spite of this, there has been very little work attempting to understand this interdependence or what impact it may have on the evolution of the Earth. We impose a mixing time in the water cycle of a thermal evolution model (Crowley et al., 2011) to understand the effects of a heterogeneous mantle water content introduced by subduction and examine the effects on the temperature, mantle water content and surface ocean evolution.

2 Methods

2.1 Evolution Model

The model is based on the Nusselt-Rayleigh relation following the procedure outlined by Crowley et al. (2011). The convective vigour is controlled by the Rayleigh number:

$$Ra = \frac{\alpha \rho g T d^3}{\kappa \eta} \tag{1}$$

where α is thermal expansivity, ρ is density, g is gravity, T is average mantle temperature, d is mantle depth, κ is thermal diffusivity and η is viscosity.

The conservation of energy

$$\frac{dT}{dt} = \frac{-Q_s + H}{\rho V c_p} \tag{2}$$

and conservation of mass

$$\frac{dX}{dt} = \frac{R - D}{\rho V} \tag{3}$$

equations are solved via the fourth order Runge-Kutta (RK4) methods where Q_s is surface heat flow, H is heating from radiogenic elements, V is mantle volume, c_p specific heat capacity, average mantle water content is X, R is regassing and D is degassing.

The conservation of energy depends on the surface heat flow, Q_s

$$Q_s = 2Sk_cT\left(\frac{U}{\pi L \kappa}\right)^{\frac{1}{2}} \tag{4}$$

and the radiogenic heat production, H

$$H = H_{sf}\sum_j \rho C_j H_j exp\left(\frac{ln2\,(t_{pd} - t)}{\tau_j}\right) \tag{5}$$

where U is plate velocity, S is surface area, k_c is thermal conductivity and L is plate length. Radiogenic heating (Eq. 5) is a sum of the contributions from U^{238}, U^{235}, Th and K

where C_j is concentration (of the j^{th} element), H_j is heat production, τ_j is radiogenic half life and t_{pd} is present day time (Table 1). Q_s is a function of U

$$U = \frac{\kappa}{d}\left(\frac{L}{\pi d}\right)^{\frac{1}{3}} Ra^{\frac{2}{3}} \tag{6}$$

and is proportional to Ra as calculated by Turcotte and Oxburgh (1967). Degassing and regassing are also a function of U:

$$D = SF_d \frac{z_m}{L} U\rho X \tag{7}$$

$$R = SF_r \frac{d_l}{L} U\rho X_p \tag{8}$$

Degassing depends on the melting depth $z_m = z_1 T_p + z_2 X + z_3$, a parametrised water-dependent melting depth (Hirschmann et al., 2009; Crowley et al., 2011) where z_1, z_2 and z_3 are constants and T_p is the potential temperature in degrees celsius (Mckenzie and Bickle, 1988). F_d and F_r are the degassing and regassing efficiencies, respectively; the values of these constants and others defined here are found in Table 2, in the Appendix. Regassing is also dependent on the thermal plate thickness $d_l = 2\left(\kappa L/U\right)^{\frac{1}{2}}$. Plate velocity is proportional to Ra as calculated by Turcotte and Oxburgh (1967).

Through the plate velocity, Q_s, R and D are all a function of Rayleigh number and hence viscosity.

2.2 Water-Dependent Viscosity

We test two simplified viscosity laws of the form

$$\eta = \eta_0 exp\left(-R_f X\right) exp\left(\frac{E}{RT}\right) \tag{9}$$

η is the viscosity, η_0 is a calibration constant, E is the activation energy, R is the ideal gas constant and R_f is the reduction factor required for the viscosity to decrease a maximum of two orders of magnitude. Of the two laws, one is water-independent ($R_f = 0$) and one is water-dependent ($R_f = 4.605 \times 10^{-3}$) with two orders of magnitude sensitivity to 1000 ppm of water. The order of magnitude variation in the water-dependent law lies in the range presented in Fei et al. (2013). Both laws are calibrated to present day Earth, average mantle conditions of 2200 K, 500 ppm water content and $5{\times}10^{21}$Pas viscosity (Figure 1).

2.3 Mixing Time

The mixing time, τ, is incorporated into the evolution model in two ways: (1) τ is constant or (2) τ is variable. Figure 3 illustrates where these steps occur with respect to solving Eqs. 2 and 3. When mixing is instantaneous i.e. $\tau = 0$, Eqs. 2 and 3 are solved using a fourth order Runge-Kutta (RK4) solver. For a constant mixing time, the water content X is found at $t_i - \tau$, hereafter $X\left[\tau\right]$. $X\left[\tau\right]$ is the value used in the RK4 solver in calculating T_{i+1} and X_{i+1} and τ is constant over the course of the model. When $t_i < \tau$, $X\left[\tau\right] = 0$ i.e. the starting mantle water content of the model.

The variable mixing time, τ_{Ra}, is calculated as

$$\tau_{Ra} = \tau \left(\frac{Ra}{Ra_{pd}} \right)^{-m} \tag{10}$$

where Ra is the Rayleigh number calculated with X_i and T_i, $Ra_{pd} = 10^6$ and $m = 2/3$ is the classical scaling between the plate velocity and Rayleigh number (Eq. 6) for any given τ. τ_{Ra} gives $X\left[\tau_{Ra}\right]$ which is the value used in the RK4 solver. In order to prevent the appearance of numerical instabilities, $X\left[\tau_{Ra}\right]$ is taken to be the average X found over five time steps, centred about τ_{Ra}.

Instantaneous mixing cases ($\tau = 0$) are calibrated by tuning the initial ocean mass to give one ocean mass ($1.39{\times}10^{21}$ kg) at the present day (4.6 Gyrs) whilst for constant and

variable mixing, mantle water content is allowed to evolve freely. By tuning H_{sf}, the surface heat flow for all models is constrained to be within the range 45 - 46 TW at the present day (Lay and Buffett, 2008). Average mantle temperature and water content evolve over the model life time with the initial temperature 2500 K, a dry mantle and a surface reservoir holding approximately two ocean masses of water.

We examine a suite of mixing times varying from 0.002 to 9 Gyrs, for constant and variable mixing and each viscosity law (Table 1).

	Symbol	$\eta(T)$	$\eta(T,X)$	Units
Surface ocean mass fraction	$M_s(t_0)$	2.04	1.94	Earth ocean masses
Radiogenic scale factor	H_{sf}	1.766	1.643	-
Viscosity calibration constant	η_0	3.77×10^{14}	3.77×10^{15}	Pas
Reduction factor	R_f	0	4.605×10^{-3}	-
Ideal gas constant	R	8.314		$\mathrm{Jmol^{-1}K^{-1}}$
Activation energy	E	3×10^5		J

Table 1: Constants for each viscosity law used to examine the effect of a water-dependent viscosity. For each viscosity law, the mixing times are also tested between 0.002 and 9 Gyrs.

3 Results

3.1 Water-Independent Viscosity

3.1.1 Instantaneous Mixing

Figure 4 shows a compilation of selected cases that represent the overall effects of a constant and variable mixing time for 9 Gyrs. The simplest case comprises of the water-independent viscosity, with $\tau = 0$, i.e. mixing is instantaneous. The mantle cools to ∼1800 K (Figure 4a) and increases in water content (Figure 4b) to ∼660 ppm. As viscosity (Figure 4c) is only dependent on temperature, the decrease in temperature causes viscosity to increase. The melting depth (Figure 4e) is dependent on both temperature and water content. As a result, during the first 2 Gyrs the change in temperature is more significant than the change in water content and the melting depth decreases with decreasing temperature. After 2 Gyrs, the change in water content is more notable than the change in temperature and melting depth increases with increasing water content. This evolution agrees with previous parametrised studies (e.g. Korenaga, 2011).

3.1.2 Constant Mixing

The addition of a constant mixing time has a pronounced effect in the water cycle as is shown in Figure 4 for a sample case of $\tau = 1$ Gyrs. The water cycle has no effect on temperature evolution as the viscosity is dependent only on temperature, hence the differences are best illustrated in Figures 4b, 4d and 4e.

During the first billion years, $X[\tau]$ is zero as no subducted water has reached a MOR (i.e. $t < \tau$). Therefore, X represents the average mantle water content and $X[\tau]$ represents the local water content at MORs. As there is no water feeding the MOR, no water is degassed during this period and the water cycle is in a state of net regassing, where more water is being subducted than is released at MORs.

Once $t > \tau$, local water content $X[\tau]$ becomes non-zero as water present in the mantle

is sampled by MORs. The increase in local water content and the corresponding increase in melting depth allows degassing to begin. Degassing increases such that it outstrips regassing and a period of net degassing is induced by ∼2 Gyrs (Figure 4b). For the remainder of the model, as $X[\tau]$ is lower than X, less water is removed than when mixing is instantaneous. This allows X to increase to above the instantaneous case by 9 Gyrs.

Net degassing causes a decrease in average mantle water content X, and after 1 Gyrs in $X[\tau]$ as well. Decreasing local water content and melting depth reduces degassing such that net regassing resumes by ∼2 Gyrs.

3.1.3 Variable Mixing

In general, the introduction of a variable mixing time using ($m = 2/3$) causes the various trends of the constant mixing case to resemble those observed for instantaneous mixing. This is the result of the dependency of mixing time on viscosity through Ra. At the beginning of the model, high temperature and low viscosity cause short mixing times, but as the mantle cools and viscosity increases, the mixing time becomes longer (Figure 4f). The period where local water content at the MOR is zero is shorter when the mixing time is variable. This is illustrated in Figure 4f by the line representing $t = \tau_{Ra}$. The variable mixing case spends less time above the line (where $X[\tau_{Ra}] = 0$) than the constant mixing case. As the mixing time increases, less water reaches MORs and therefore less water can be degassed. This results in the absence of a period of net degassing and more water residing in the mantle for variable mixing than instantaneous mixing.

3.1.4 Influence of Mixing Time Scaling

The data presented in Figure 4 was calculated using the scaling relationship $\tau_{Ra} \propto Ra^{-m}$ where $m = 2/3$. To test the effect this scaling has on mantle evolution, we vary m from 0 to 1, where $m = 0$ is equivalent to a constant mixing time. The results are shown in Figure 5. As with Figure 4, the temperature (Figure 5a) and viscosity (Figure 5c) are the same for

each case. As m is increased, $\tau_{Ra}(t=0)$ decreases (Figure 5f), and for $m=1$, the unscaled mixing time, τ, of 1 Gyrs is reduced by two orders of magnitude to 0.01 Gyrs. This decreases the period where $X\left[\tau_{Ra}\right]=0$ in which the mantle goes through fluctuations in water content and an early period of degassing; and ceases where mixing time is strongly dependent on Ra ($m \gtrsim 0.6$), in which water content increases smoothly and no period of degassing occurs. It is notable that the threshold value of $m \approx 0.6$ is close to the value of $m = 2/3$ predicted from the simple subduction model described in Figure 1.

For cases in which m is small (τ_{Ra} is weakly dependent on Ra), the initial period of net regassing is longer, leading to a greater build up of water in the mantle early on: for $m=0$, X reaches a local maximum of 588 ppm at 1.5 Ga. This excess of water eventually leads to a period of net degassing, lasting from 1.5 Ga to 3.2 Ga. For cases with a slightly larger m (mixing time is more sensitive to Ra), the period of initial net regassing and the period of net degassing as the mantle readjusts become shorter, until by $m=0.6$ there is no maxima in X and no period of degassing. The duration of the degassing period and its dependence on m will be discussed further in Section 4.1.

These cases may thus be divided into two sets: cases where mixing time is weakly dependent on Ra ($m < 0.6$) with a period of net degassing and cases where mixing time is strongly dependent on Ra ($m \geq 0.6$) where there is no period of net degassing.

3.2 Water-dependent Viscosity

3.2.1 Instantaneous Mixing

Figure 6, shows representative cases with a viscosity law that also depends on water content (Eq. 9). The simplest case for a water-dependent rheology is also when mixing is instantaneous, i.e. $\tau = 0$. Over 9 Gyrs, the mantle cools to $\sim$ 1700 K (Figure 4a) and water content increases to $\sim$ 670 ppm. The thermal evolution exhibits a short period of initial heating for $\sim$ 0.2 Gyrs because the model starts with a dry (and therefore viscous) mantle. By starting with a stiffer mantle, convection is less vigorous, therefore surface heat

flow (Eq 4) is reduced and radiogenic heat (Eq. 5) becomes dominant, causing a period of heating. During this time, water is being subducted into the mantle (Figure 6b) and the increase in both temperature and water content contribute to a decrease in viscosity (Figure 6c) and increase in melting depth (Figure 6d). The decrease in viscosity allows surface heat flow to increase until it becomes greater than radiogenic heating and the mantle cools. The increase in melting depth and water content during the period of heating increases degassing. However, regassing remains dominant and the water cycle is in a state of net regassing for the entirety of the model.

3.2.2 Constant Mixing

Implementation of a constant mixing time has a similar effect as when viscosity is water-independent. Some of the extreme variations in the mixing depth and other properties that were seen in the water-independent case have been damped; for constant mixing, the peak water content in the early Earth ($t < 4$ Ga) is 453 ppm, compared to 588 ppm in the water-independent case (Figure 4e). The oscillations in water content are associated with changes in the viscosity (Figure 6c) and therefore also affect mantle temperature (Figure 6a), which both exhibit fluctuations for $t < 6$ Ga.

During the first billion years when $X[\tau] = 0$, heating is more pronounced than in the instantaneous mixing case. The water subducted during this time has not reached a MOR and therefore, surface heat flow is only dependent on temperature as before. The mantle feeding MORs is dry, local viscosity is relatively high and surface heat flow is lower than radiogenic heating. The mantle heats faster than for the instantaneous case causing viscosity to decrease. This allows surface heat flow to increase until it becomes greater than radiogenic heating and the mantle begins to cool.

After 1 Gyrs, $X[\tau] > 0$ and water subducted at the start of the model reaches the MOR. The increase in $X[\tau]$ (local water content) decreases local viscosity at the MOR, increasing the surface heat flow and causing a period of rapid cooling. Increasing X (Figure 6b) and

decreasing temperature counter-act each other such that melting depth and viscosity change little over this period.

Decreasing $X\,[\tau]$ (Figure 6e) at ~ 2.5 Gyrs increases local viscosity such that surface heat flow is slowed and temperature becomes stable. Melting depth (Figure 6d) decreases by $\sim$ 50 km as the local water content decreases. This reduces degassing and net regassing occurs for the remainder of the model.

3.2.3 Variable Mixing

The final layer of complexity comes with the inclusion of a variable mixing time. As with a water-independent viscosity, variable mixing closely resembles instantaneous mixing where a shorter mixing time at the beginning of the model causes a shorter period in which $X\,[\tau_{Ra}] = 0$ (Figure 6e and 6f). Less water is subducted and net degassing is no longer induced. However, unlike the water-independent case, mantle water content (Figure 6b) exhibits stability for 0.2 Gyrs, which suggests that varying the mixing time before it is scaled by Ra may cause net degassing to reappear for τ other than 1 Gyr (Eq. 10). Differences in local viscosity and temperature evolution are also more comparable to those when mixing is instantaneous as the effects of degassing are dampened by variable mixing.

3.2.4 Influence of Mixing Time Scaling

Varying m when viscosity is water-dependent has similar effects as when examining the differences seen in Figures 4 and 6; the initial scaled mixing time (Figure 7f) has a range of one order of magnitude with $m = 1$ resulting in 0.1 Gyrs. This dampening effect of the water-dependent viscosity results in less extreme behaviour. As with Figure 6, there is also a feedback to the temperature (Figure 7a) and viscosity (Figure 7c) evolution. As with the water-independent case (Figure 5), a period of net degassing is induced for $m \leq 0.5$, showing that if the mixing time does not vary by orders of magnitude, net degassing is expected.

In summary, for a mixing time of 1 Gyrs, constant mixing ($m = 0$) induces a period of

net degassing whilst variable mixing dampens that effect and resembles the instantaneous case (for $m > 0.6$). A constant mixing time assumes subducted water takes 1 Gyrs to reach a MOR. This leads to an early build up of water in the mantle and a period of degassing as the mantle readjusts. In contrast, for cases where the mixing time is strongly dependent on Ra (i.e. for $m \gtrsim 0.6$), the greater mantle temperatures in the early Earth ensure that τ_{Ra} is very small for much of Earth's history and as a result the mantle evolution closely resembles that seen for the instantaneous mixing case.

As the model progresses ($t \gtrsim 4$ Ga), the trends in the water content (Figure 6b) and temperature (Figure 6a) converge, with the exception of the instantaneous mixing case ($m = 0$). This indicates that even a weak dependence of mixing time on mantle conditions (i.e. Ra) is sufficient to cause the mantle evolution in the present day to resemble the idealised case of instantaneous mixing.

The mantle evolution is most sensitive to the mixing time in the early Earth; this is unsurprising, given this is the period in which changes in Ra are most rapid. The mantle evolution appears to be very sensitive to the mixing time at $t = 0$, as this can lead to a build up of large quantities of water in the mantle followed by a period of degassing (Figure 6b), highlighting the importance of initial conditions in the mantle for the evolution of the planet.

4 Discussion

4.1 Periods of Net Degassing

In Figures 4 - 7, we present only the cases of mixing where $\tau = 1$ Gyrs. However, estimates for the present day mixing time for Earth vary from a few hundred million years to a few billion years (Kellogg and Stewart, 1991; Samuel et al., 2011). This will inevitably have an impact on the transitions between regassing and degassing in the water cycle presented in the previous section.

When a mixing time is present, the water cycle can go through three phases: (1) initial net regassing when $X\left[\tau_{(Ra)}\right] = 0$, (2) net degassing when $X\left[\tau_{(Ra)}\right]$ initially becomes non-zero and (3) net regassing for the remainder of the model. These timings can be examined by extracting the turning points of X. These points represent where $\frac{dX}{dt} \sim 0$, i.e. when net degassing begins or ends. Figure 8 presents data from the four different suites of models (constant and variable mixing for both water-independent and water-dependent viscosity laws) considered in the previous section, but here τ varies between 0.002 and 9 Gyrs. Cases with variable mixing times were performed using $m = 2/3$. Figure 8a shows the constant mixing time case for a water-independent viscosity where there are two turning points; the first indicates the start of net degassing and the second indicates the end of net degassing. For $\tau < 0.2$ Gyrs, there are no turning points and the water cycle is always in a state of net regassing, behaving almost identically to the instantaneous mixing case. For $\tau > 0.2$ Gyrs we see the beginning and end of a net degassing period. In general, as the mixing time increases, both the start and end of net degassing are delayed and the duration of net degassing increases. The first turning points follow a linear trend as the onset of water's influence on degassing is controlled by the end of the period where $X[\tau]$ is zero. The end points follow a linear trend until after 2 Gyrs where end times appear to deviate.

Figure 8b shows two suites of data for constant mixing and a water-dependent viscosity. The dashed outline encloses the area of degassing when the surface heat flow does not

fall between the required 45 - 46 TW. The net degassing region looks similar to the water-independent viscosity case (Figure 8a) with the period starting later and ending earlier. However, when the surface heat flow condition is met, the region is irregular lying approximately within the outlined region. This scaling (values in Table 3 of the Appendix) further shortens the duration of net degassing.

The addition of a variable mixing time has a drastic impact on net degassing. For a water-independent viscosity shown in Figure 8c, a period of net degassing only occurs for τ = 2 - 3 Gyrs lasting $\sim$ 0.4 - 1 Gyrs, respectively. In contrast, for the same period in constant mixing, net degassing lasts $\sim$ 3 - 4 Gyrs, respectively. The period also occurs much earlier for variable mixing starting $\sim$ 0.5 - 1 Gyrs when τ = 2 - 3 Gyrs compared with $\sim$ 2.7 - 4 Gyrs for constant mixing, respectively. Hence, a variable mixing time causes net degassing to occur earlier and for a much shorter period, i.e. the start occurs later and the end occurs earlier, and only for a limited range of τ.

When viscosity is dependent on water and the mixing time is variable (Figure 8d), net degassing occurs when the mixing time is between 1.5 and 2.5 Gyrs lasting $\sim$ 0.25 - 0.37 Gyrs. As with constant mixing, the inclusion of a water-dependent viscosity narrows the region of net degassing. However, net degassing is still possible in a mixing time interval of 1 Gyrs, although it occurs for a slightly lower range of τ= 1.5 - 2.5 Gyrs, compared to 2 - 3 Gyrs for the water-independent viscosity (Figure 6c). These results demonstrate how the existence and duration of a period of degassing is very sensitive to both the mantle viscosity and the estimates of the mantle mixing time.

When exploring the influence of mixing time, the inverse relationship is seen. For example, Figure 9a shows periods of net degassing as a function of m in Eq. 10 for $\eta(T, X)$ (Figure 7). Increasing m decreases the time period when $t < \tau_{Ra}$, therefore less water is solely regassed and the later influence on melting depth is not as evident. Mixing becomes more dependent on mantle conditions as m increases and as result, net degassing occurs earlier and lasts for a shorter period of time.

By varying both τ_{Ra} and m, behaviour in the first $\sim$4 Gyrs is dominated by evolution in the first few hundred million years. This implies that the history of the the mantle water content and surface ocean is very sensitive to the initial mixing conditions.

4.2 Surface Ocean Volume

Figure 9b shows the surface ocean volume at 4.6 Gyrs of each case examined in Figure 8. When the surface ocean is zero, all the water has been subducted into the mantle ($\sim$ 2 oceans).

The majority of cases show less water at the surface at 4.6 Gyrs than for the instantaneous mixing case, i.e. where $\tau = 0$. For most cases, as the mixing time increases, the surface ocean volume decreases. Deviations from these features are between 0.8 and 4 Gyrs for Figure 9a. These cases finish during or soon after the end of a period of net degassing. As net degassing lowers average mantle water content X, more water is found in the surface reservoir. These cases can end with a larger surface ocean than the instantaneous case. Even if these cases have gone through the end of net regassing, it still takes time for water content to recover and to be returned to the mantle. Therefore, cases that do not finish in a state of net degassing can still feel the effects of this period.

Constant mixing cases (orange in Figure 9b) can show high surface ocean volumes in comparison to the instantaneous case. Periods of net degassing are longer allowing more water to be released to the surface reservoir, resulting in less water in the mantle. When mixing is variable and the viscosity law is also water-dependent the surface ocean volume decreases and the effect of net degassing in the few cases where it does occur, is negligible. It is clear from Figure 9b, that when mixing is included, variations in the surface ocean mass and hence the average mantle, can be on the order of oceans. In general, as the mixing time is increased, the size of the surface ocean diminishes, unless the model is in a state of net degassing or is still recovering from one.

4.3 Physical Interpretation and Implications

It is clear that the incorporation of mixing time into the parametrised model has a large effect on the water content and thermal evolution and can lead to extended periods of net degassing. The mixing time effectively means that it takes a finite amount of time for water to reach a MOR after being subducted and hence there is a period where water cannot influence degassing or be degassed. The mixing time represents an average for all paths that water can travel from the subduction zone to reach a MOR and assumes that no water is permanently locked away at depth. All surface water is subducted into the mantle by 9 Gyrs for most cases as melting and hence degassing become inefficient with decreasing mantle temperature. As the mixing time increases, mixing becomes more and more inefficient and it takes longer for water to reach a MOR. Less water is available to be degassed, trapping water at depth and keeping the mantle in a state of net regassing.

The models presented are particularly efficient in their temperature evolution and are much cooler by 4.6 Gyrs than current estimates for the Earth's mantle (Condie et al., 2016). This is the result of a convecting system based on plate tectonics, which is an extremely efficient way to transport water and heat between the surface and interior. Whilst suppressed cooling as a result of incorporating a mixing time into the model may contribute to keeping the mantle hotter by tens of degrees, this suggests that Earth-like temperature conditions of ~ 2200 K are a result of more complex, large scale processes such as changes in convective regime (Korenaga, 2011). The effects of mixing are evident in the water cycle whilst the impact on the temperature evolution is more subtle, especially for variable mixing with a water-dependent viscosity, implying that there is a limited effect of mixing on the temperature evolution. Variations in temperature at 4.6 Gyrs are < 50 K with the exception of cases with constant mixing, water-dependent viscosity and $\tau_{Ra} > 1.5$ Gyrs where temperatures can vary between 1800 and 2100 K.

The cases presented are in agreement with others (e.g. Korenaga et al., 2017; Nakagawa and Spiegelman, 2017) where net regassing dominates. However, unlike previous paramet-

rised models, we start with a large surface ocean rather than a hydrous mantle (Crowley et al., 2011; Sandu et al., 2011). This results in the loss of an initial degassing phase that stiffens the mantle and induces heating, although heating is still induced by the lack of water in the mantle at the beginning of the model. Cases with variable mixing are also in agreement with previous models where the mantle is not only hotter, but drier in the past, particularly during 0.5 and 2 Gyrs, corresponding to the Archean for Earth. As the planet has cooled, mixing time increases with decreasing Ra and the propensity to degas the mantle reservoir diminishes.

Mixing has the greatest effect on temperature and water evolution when viscosity is independent of water content. Even if viscosity is not dependent on water (Muir and Brodholt, 2018), it still influences the melting depth which can have large implications for the overall evolution by inducing a state of net degassing whilst a water-dependent viscosity acts to shorten this period. Present day mixing times from geochemistry vary from $\sim$ 0.5 - 2 Gyrs (Gonnermann and Mukhopadhyay, 2009) and up to $\sim$ 1 Gyrs from geodynamic models (Tackley, 2015). But for early Earth, Hadean mixing times on the 0.1 Gyrs scale is predicted from models with a mobile lid, i.e. plate tectonics (e.g. Samuel et al., 2011; Kellogg and Stewart, 1991) whilst geochemistry predicts the survival of reservoirs for $\sim$ 2 Gyrs (O'Neill et al., 2013). Mixing in a stagnant lid model by O'Neill et al. (2013) suggests mixing operates on timescales more comparable to the present day. Whilst there is uncertainty in mixing style (constant or variable) and the sensitivity of the mantle viscosity to water content (negligible or up to three orders of magnitude), it is clear that the delayed effect of water on melting depth at mid-ocean ridges can cause significant changes in the water cycle. This suggests that the effect of water on the melting depth coupled with mixing may be more important than its relationship with viscosity when considering whole mantle evolution. The melting depth also varies across over the course of the model. Greater depths in the past allow degassing to become prevalent in cases that show net degassing but this also has geochemical implications, causing variations in the geochemistry of the basaltic crust.

These changes induced by the lag between regassing during subduction and degassing at MORs also has an effect on the surface reservoir (Figure 9b). As little as 1 ppm can cause an increase in today's global-mean sea level of 10 m, indicating a significant contribution of mantle water to changes in sea level even if changes in the surface reservoir are on the order of a few ppm. Figure 9b shows that these changes occur over hundreds of millions or billions of years. Today, global-mean sea level is rising at a rate of $\sim$ 3 mm/yr (Watson et al., 2015) whereas changes in the constant mixing case (Figure 4) are of the order 10^{-3} mm/yr. On short timescales, the mantle water contribution may not have much of an impact compared to ice sheet formation and other factors but over the evolution of the Earth would causes significant changes in the surface ocean volume and water content of the mantle. Even with lower estimates of mixing time (<1 Gyrs), changes in surface ocean mass can be of up to 0.1 ocean masses, which would change sea level by $\sim$ 400 m. During the initial phase of net regassing, the surface ocean diminishes and loses $\sim$ 600 ppm, equivalent to a drop in sea level of 6 km, which could easily uncover highs in the sea floor. For the Earth, we can consider the onset of plate tectonics $\sim$ 2.5 Ga. If we assume that this is also the beginning of the relatively efficient transport of water into the deep mantle, topography could easily become uncovered and enhance subaerial weathering, an important process aiding the formation of continental crust (Höning et al., 2014).

5 Conclusions

We present a parametrised model (Crowley et al., 2011) adapted to include the coupled effects of mixing and a water-dependent viscosity to explore the effects of mixing on mantle water content and surface ocean volume. The introduction of a second water content $X\left[\tau_{(Ra)}\right]$ results in degassing controlled by a local water content, different from the average mantle water content. This results in a period of net degassing where mantle water content decreases and the surface ocean volume increases. The impact of water on melting depth facilitates the appearance of a net degassing period, having a larger effect on the overall water cycle evolution than a water-dependent viscosity. Whilst $\eta(T, X)$ shortens the period of net degassing, a variable mixing time coupled to mantle conditions can prevent this period from occurring at all. The inclusion of mixing reduces the size of the surface ocean, increasing mantle water content with even the smallest variation resulting in 10's of metres difference in sea level.

Acknowledgements

This work was funded by NERC as part of the Deep Volatiles Consortium (NE/M00046X/1).

References

Kent C. Condie, Richard C. Aster, and Jeroen van Hunen. A great thermal divergence in the mantle beginning 2.5 Ga: Geochemical constraints from greenstone basalts and komatiites. *Geoscience Frontiers*, 7(4): 543–553, jul 2016. ISSN 16749871. doi: 10.1016/j.gsf.2016.01.006. URL http://linkinghub.elsevier.com/retrieve/pii/S1674987116000311.

John W Crowley, Mélanie Gérault, and Richard J O'Connell. On the relative influence of heat and water transport on planetary dynamics. *Earth and Planetary Science Letters*, 310(3-4):380–388, 2011. doi: 10.1016/j.epsl.2011.08.035.

H Fei, M Wiedenbeck, D Yamazaki, and T Katsura. Small effect of water on upper-mantle rheology based on silicon self-diffusion coefficients. *Nature*, 498(7453):213–215, 2013. doi: 10.1038/nature12193. URL http://www.ncbi.nlm.nih.gov/pubmed/23765497.

Helge M. Gonnermann and Sujoy Mukhopadhyay. Preserving noble gases in a convecting mantle. *Nature*, 459(7246):560–563, may 2009. ISSN 0028-0836. doi: 10.1038/nature08018. URL http://www.nature.com/articles/nature08018.

Marc M. Hirschmann, Travis Tenner, Cyril Aubaud, and A. C. Withers. Dehydration melting of nominally anhydrous mantle: The primacy of partitioning. *Physics of the Earth and Planetary Interiors*, 176(1-2):54–68, 2009. ISSN 00319201. doi: 10.1016/j.pepi.2009.04.001.

Dennis Höning and Tilman Spohn. Continental growth and mantle hydration as intertwined feedback cycles in the thermal evolution of Earth. *Physics of the Earth and Planetary Interiors*, 255:27–49, jun 2016. ISSN 00319201. doi: 10.1016/j.pepi.2016.03.010. URL http://linkinghub.elsevier.com/retrieve/pii/S0031920116300103.

Dennis Höning, Hendrik Hansen-Goos, Alessandro Airo, and Tilman Spohn. Biotic vs. abiotic Earth: A model for mantle hydration and continental coverage. *Planetary and*

Space Science, 98:5–13, aug 2014. ISSN 00320633. doi: 10.1016/j.pss.2013.10.004. URL http://linkinghub.elsevier.com/retrieve/pii/S0032063313002663.

Louise H. Kellogg and Cheryl a. Stewart. Mixing by chaotic convection in an infinite Prandtl number fluid and implications for mantle convection. *Physics of Fluids A: Fluid Dynamics*, 3(5):1374, 1991. ISSN 08998213. doi: 10.1063/1.858067. URL http://scitation.aip.org/content/aip/journal/pofa/3/5/10.1063/1.858067.

J Korenaga. Thermal evolution with a hydrating mantle and the initiation of plate tectonics in the early Earth. *Journal of Geophysical Research*, 116(B12): B12403, dec 2011. ISSN 0148-0227. doi: 10.1029/2011JB008410. URL http://doi.wiley.com/10.1029/2011JB008410.

Jun Korenaga, Noah J. Planavsky, and David A. D. Evans. Global water cycle and the coevolution of the Earth's interior and surface environment. *Philosophical Transactions of the Royal Society A: Mathematical, Physical and Engineering Sciences*, 375(2094):20150393, 2017. ISSN 1364-503X. doi: 10.1098/rsta.2015.0393. URL http://rsta.royalsocietypublishing.org/lookup/doi/10.1098/rsta.2015.0393.

Thorne Lay and Bruce Buffett. Core â mantle boundary heat flow. *Nature Geoscience*, pages 13–15, 2008. ISSN 1752-0894. doi: 10.1038/ngeo.2007.44.

D. Mckenzie and M. J. Bickle. The volume and composition of melt generated by extension of the lithosphere. *Journal of Petrology*, 29(3):625–679, 1988. ISSN 00223530. doi: 10.1093/petrology/29.3.625.

S. Mei and D. L. Kohlstedt. Influence of water on plastic deformation of olivine aggregates: 1. Diffusion creep regime. *Journal of Geophysical Research*, 105:21457, 2000. ISSN 0148-0227. doi: 10.1029/2000JB900179.

Joshua M.R. Muir and John P. Brodholt. Water distribution in the lower mantle: Implications for hydrolytic weakening. *Earth and Planetary Science Let-*

ters, 484:363–369, 2018. ISSN 0012821X. doi: 10.1016/j.epsl.2017.11.051. URL http://linkinghub.elsevier.com/retrieve/pii/S0012821X17306957.

Takashi Nakagawa and Marc W. Spiegelman. Global-scale water circulation in the Earth's mantle: Implications for the mantle water budget in the early Earth. *Earth and Planetary Science Letters*, 464:189–199, 2017. ISSN 0012821X. doi: 10.1016/j.epsl.2017.02.010. URL http://dx.doi.org/10.1016/j.epsl.2017.02.010.

Takashi Nakagawa, Tomoeki Nakakuki, and Hikaru Iwamori. Water circulation and global mantle dynamics: Insight from numerical modeling. *Geochemistry, Geophysics, Geosystems*, 16(5):1449–1464, 2015. doi: 10.1002/2014gc005701.

Craig O'Neill, Vinciane Debaille, and William Griffin. Deep earth recycling in the Hadean and constraints on surface tectonics. *American Journal of Science*, 313(9):912–932, nov 2013. ISSN 0002-9599. doi: 10.2475/09.2013.04. URL http://www.ajsonline.org/cgi/doi/10.2475/09.2013.04.

H. Samuel, V. Aleksandrov, and B. Deo. The effect of continents on mantle convective stirring. *Geophysical Research Letters*, 38(4):1–5, 2011. ISSN 00948276. doi: 10.1029/2010GL046056.

Constantin Sandu, Adrian Lenardic, and Patrick McGovern. The effects of deep water cycling on planetary thermal evolution. *Journal of Geophysical Research: Solid Earth*, 116(12): 1–16, 2011. ISSN 21699356. doi: 10.1029/2011JB008405.

Johnny Seales and Adrian Lenardic. Deep Water Cycling and Delayed Onset Cooling of the Earth. jan 2018. URL http://arxiv.org/abs/1801.09148.

P.J. Tackley. Mantle Geochemical Geodynamics. In *Treatise on Geophysics*, volume 7, pages 521–585. Elsevier, 2015. ISBN 9780444538031. doi: 10.1016/B978-0-444-53802-4.00134-2. URL http://dx.doi.org/10.1016/B978-0-444-53802-4.00134-2 http://linkinghub.elsevier.com/retrieve/pii/B9780444538024001342.

D L Turcotte and E R Oxburgh. Finite amplitude convective cells and continental drift. *Journal of Fluid Mechanics*, 28(01):29–42, apr 1967. ISSN 0022-1120. doi: 10.1017/S0022112067001880. URL http://www.journals.cambridge.org/abstract_S0022112067001880.

Christopher S. Watson, Neil J. White, John A. Church, Matt A. King, Reed J. Burgette, and Benoit Legresy. Unabated global mean sea-level rise over the satellite altimeter era. *Nature Climate Change*, 5(6):565–568, jun 2015. ISSN 1758-678X. doi: 10.1038/nclimate2635. URL http://www.nature.com/articles/nclimate2635.

Figures

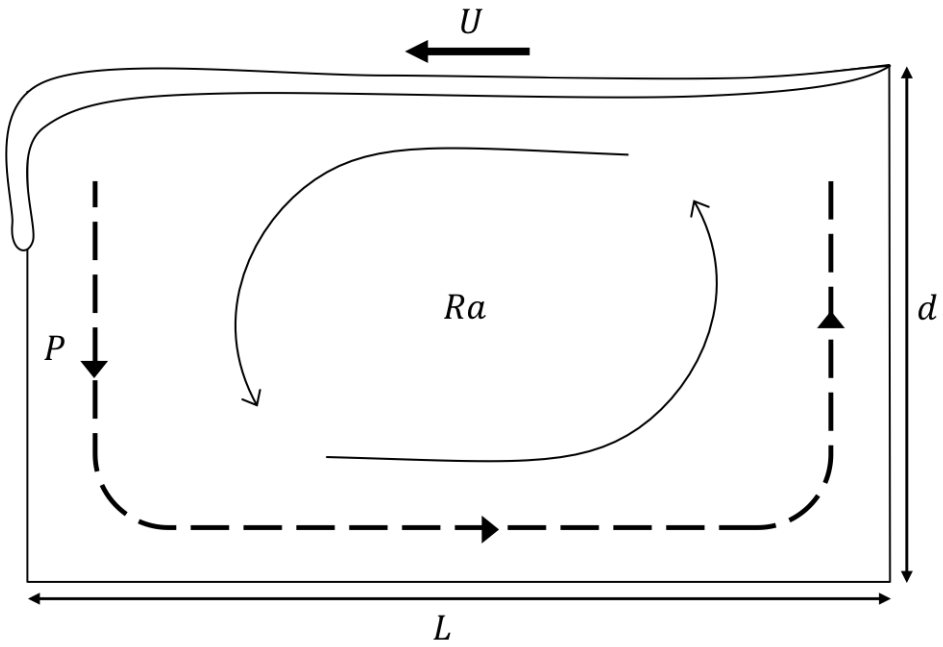

Figure 1: The path, P, from subduction zone to mid-ocean ridge (MOR) represents the path of a subducting package. The time for the package to travel along this path is the mixing time, τ, proportional to the convective vigour, Ra and hence temperature and water content through viscosity.

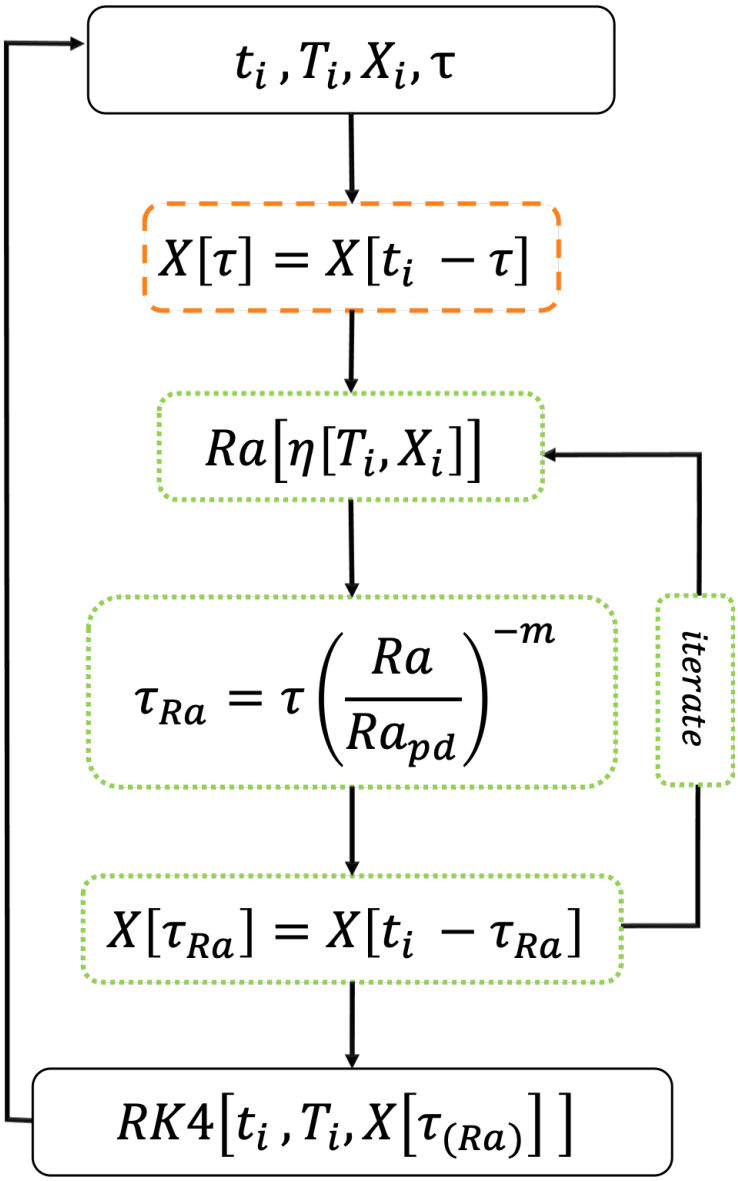

Figure 2: COLOUR Viscosity variation with respect to water content at 2200 K for both viscosity laws used in this model from Eq 9. The previous viscosity law implemented by Crowley et al. (2011) is shown for comparison. The water-dependent law, $\eta(T, X)$, is calibrated to $5{\times}10^{21}$ Pas at 500 ppm and varies one order of magnitude for up to 1000 ppm.

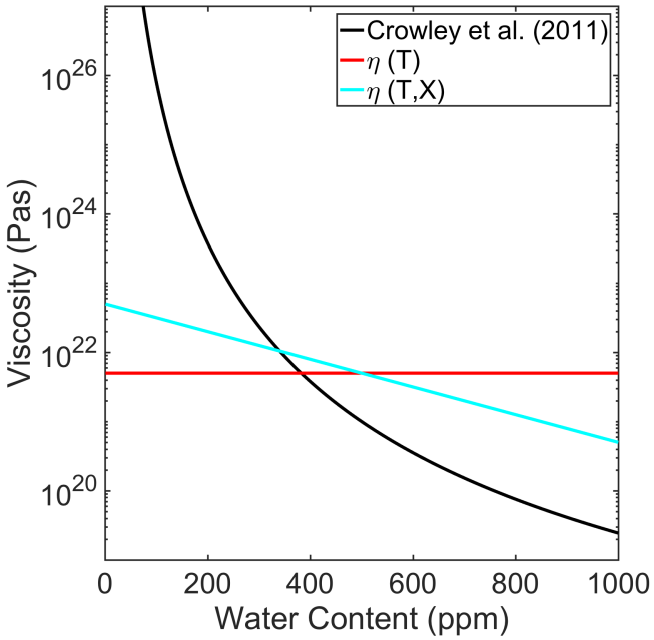

Figure 3: COLOUR Schematic representing the main calculation loop. Solid boxes represent the steps taken in all cases, the orange dashed box represents the additional step when mixing time is constant and green, dotted boxes represents the steps when mixing time is variable. τ is the constant mixing time or when mixing is variable, it is the prescribed mixing time that is later scaled by Ra to give τ_{Ra}. Equations 2 and 3 are solved with a fourth order Runge-Kutta solver, RK4 with $X\left[\tau_{(Ra)}\right]$ and hence the evolution is dependent on $X\left[\tau_{(Ra)}\right]$.

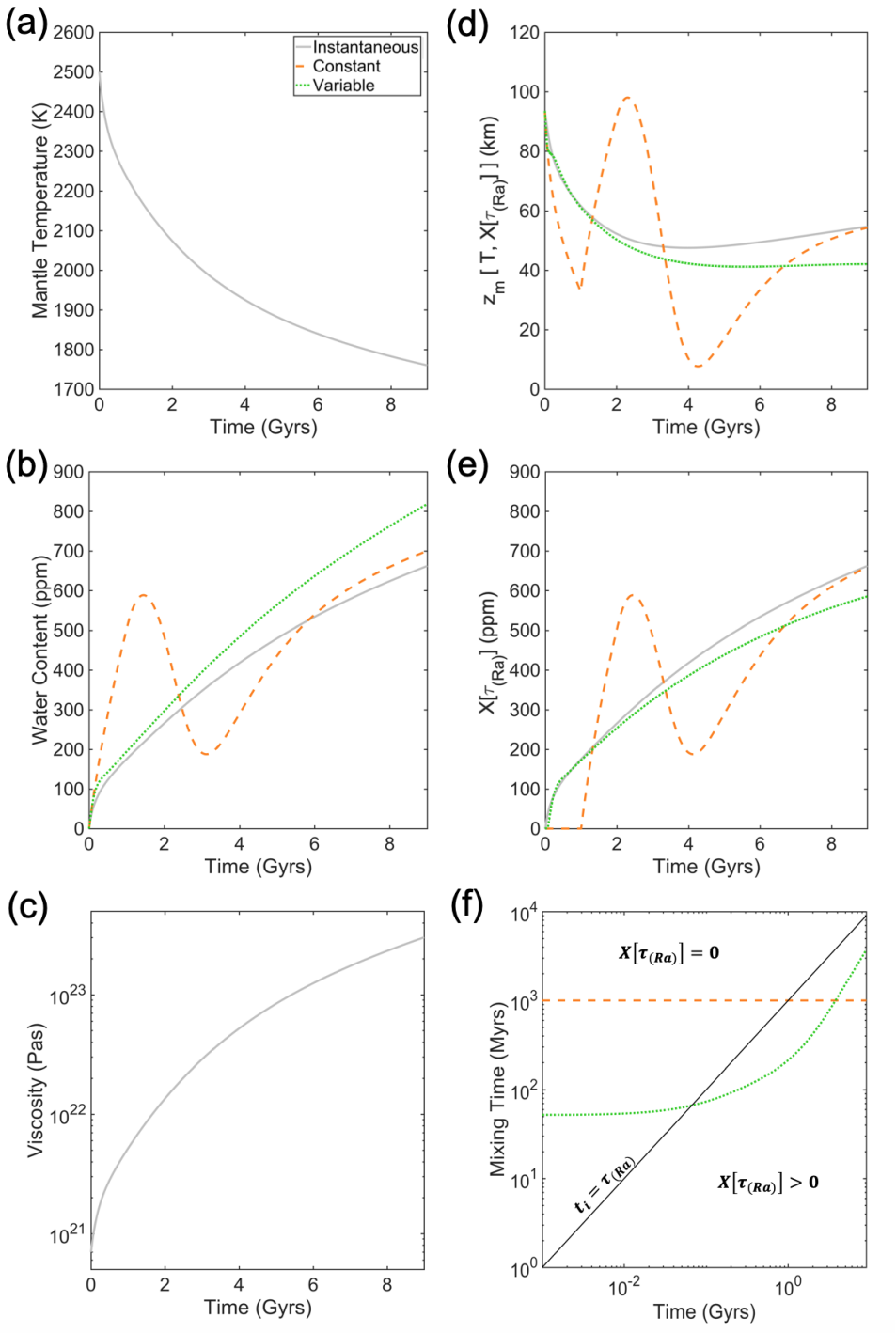

Figure 4: COLOUR Representative cases of a temperature-dependent viscosity law with various mixing implementations The panel consist of the parameters that affect evolution the most: (a) mantle temperature T , (b) water content X , (c) viscosity, (d) water content at $t_i - \tau_{(Ra)}$, (e) melting depth and (f) mixing time . Line style shows how evolution changes with respect to style of mixing. Temperature and viscosity evolution are identical for all three mixing cases as rheology is only temperature-dependent. The solid black line in (f) represents the line above which $X\left[\tau_{(Ra)}\right] = 0$ and below $X\left[\tau_{(Ra)}\right] > 0$ as defined in (d).

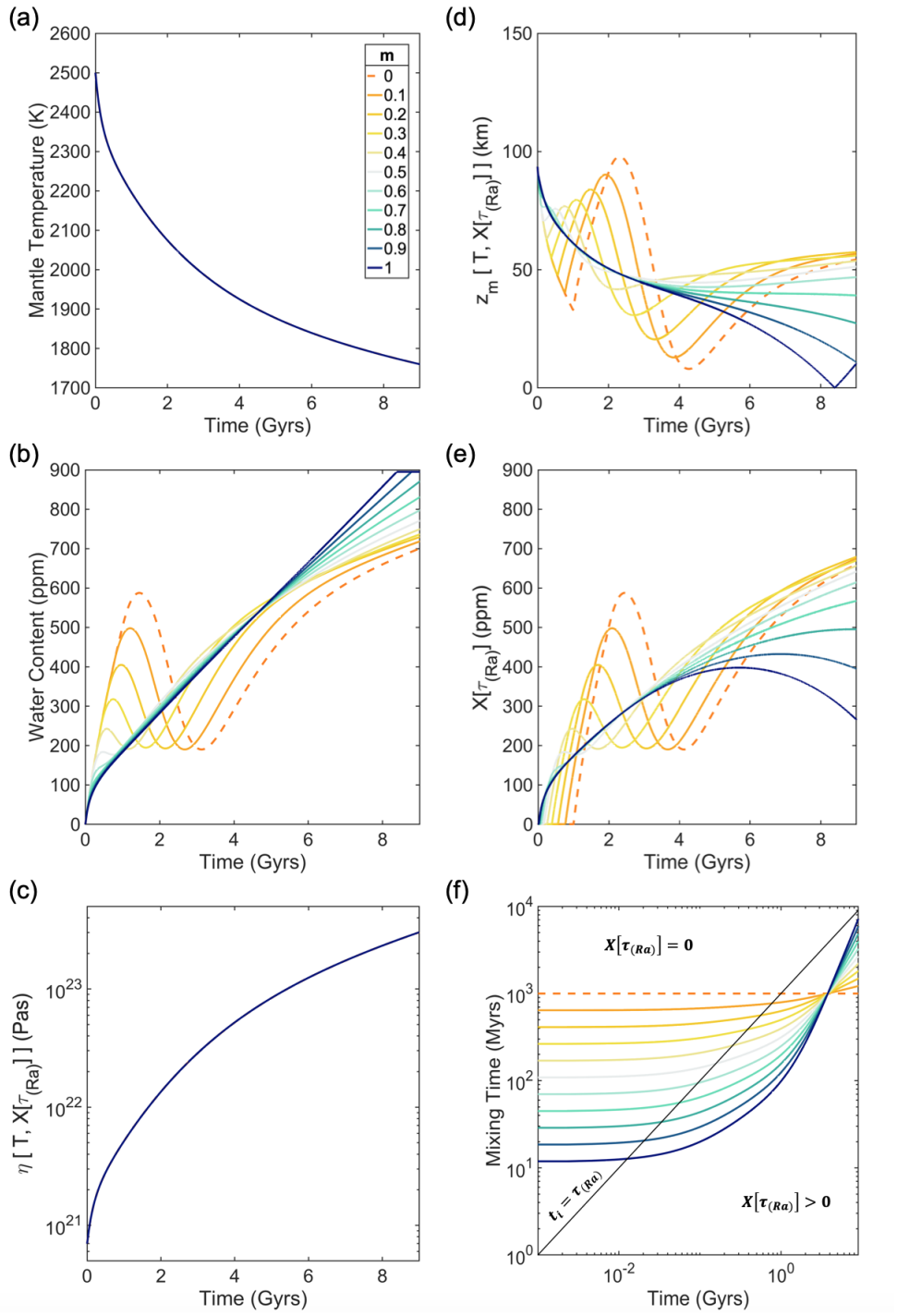

Figure 5: COLOUR Variation in evolution due to changing m-exponent in the variable mixing time relationship for a water-dependent viscosity. (a) average mantle temperature, (b) average mantle water content, (c) average mantle viscosity, (d) melting depth, (e) local water content at MOR and (f) mixing time. $m = 0$ (dashed orange) represents the constant mixing case also presented in Figure 4 and dark blue represents $m = 1$. As the exponent increases, shorter mixing times are achieved at the beginning of the model. This decreases the time the model spends with only regassing operating, removing the period of net degassing and increasing the water content of mantle.

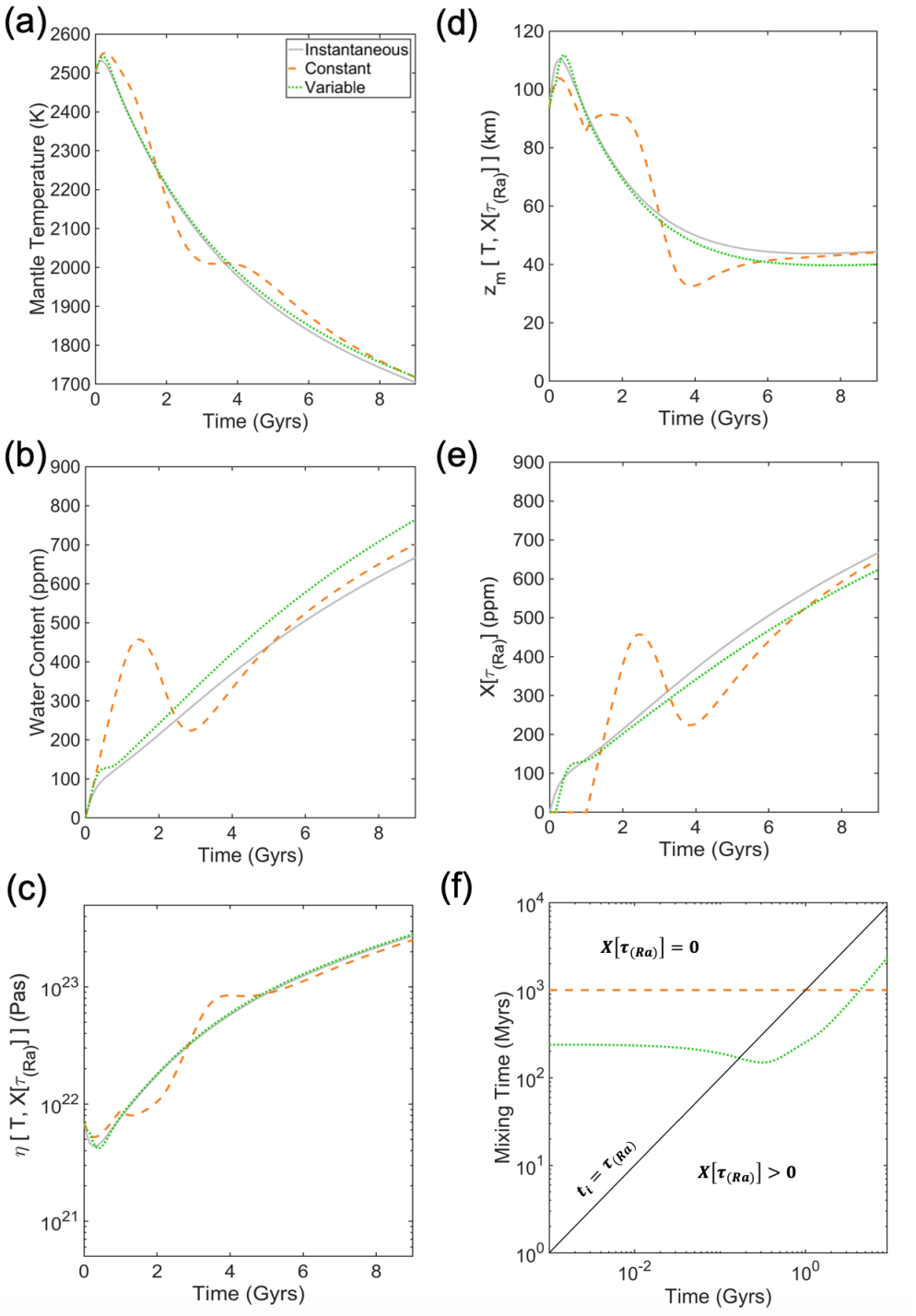

Figure 6: COLOUR Representative cases of a water-dependent viscosity with various mixing implementations where $\tau = 1$ Gyrs for both constant mixing and variable mixing (before being scaled by Ra). (a) is average mantle temperature and (b) is average mantle water content. When mixing is instantaneous, (c) represents the average mantle viscosity and when mixing is included (constant or variable), (c) represents the local viscosity at the MOR. (d) is the melting depth, (e) is local water content at the MOR and (f) is the mixing time. Overall, the results are similar to those of the water independent case shown in Figure 4, but the periods of degassing are somewhat damped.

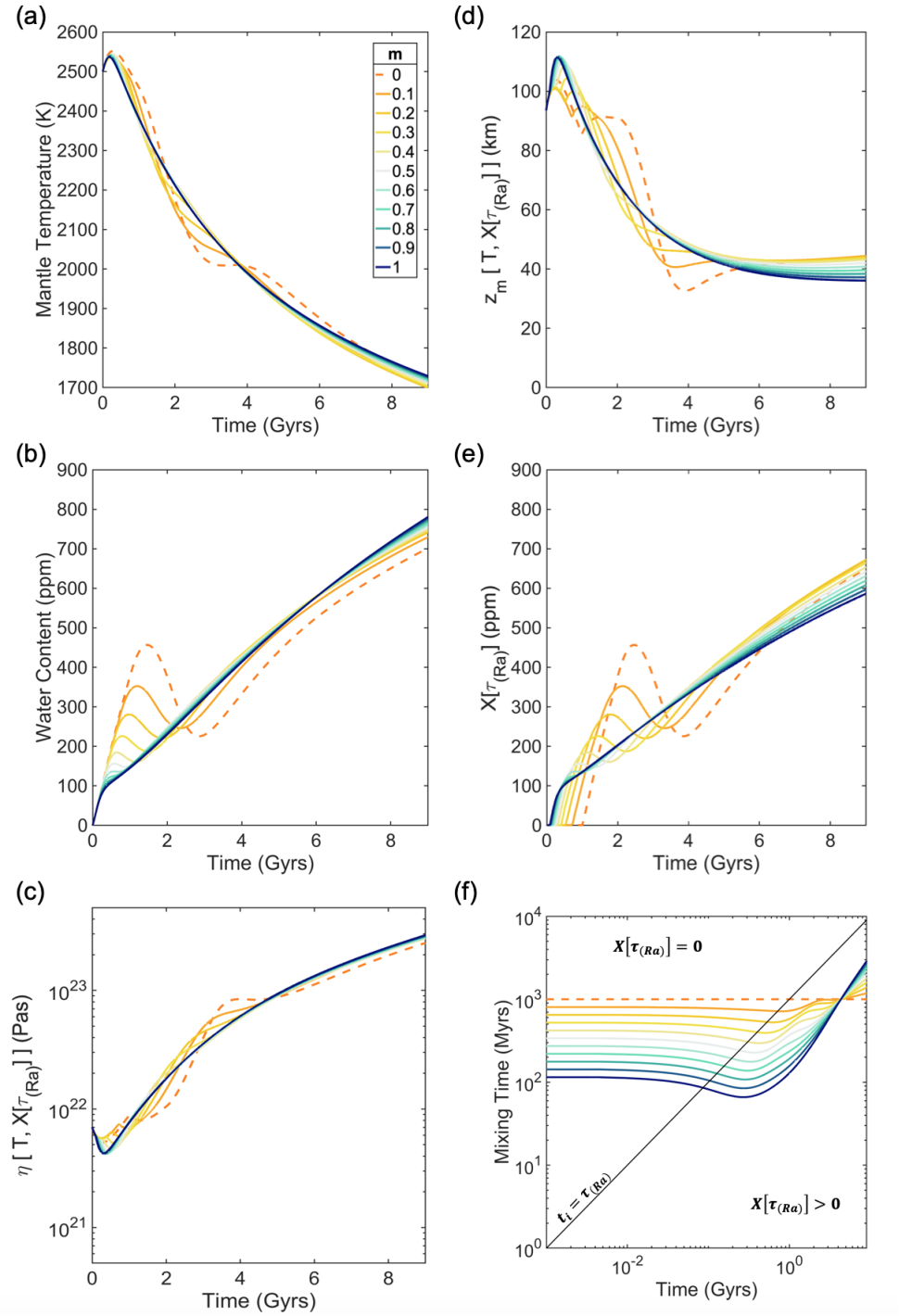

Figure 7: COLOUR Variation in evolution due to changing m-exponent in the variable mixing time relationship for a water-dependent viscosity. $m = 0$ represents the constant mixing case. The results are similar to those of the water independent viscosity shown in Figure 5, although the water-dependent viscosity tends to dampens the extreme regassing and degassing near the start of the model.

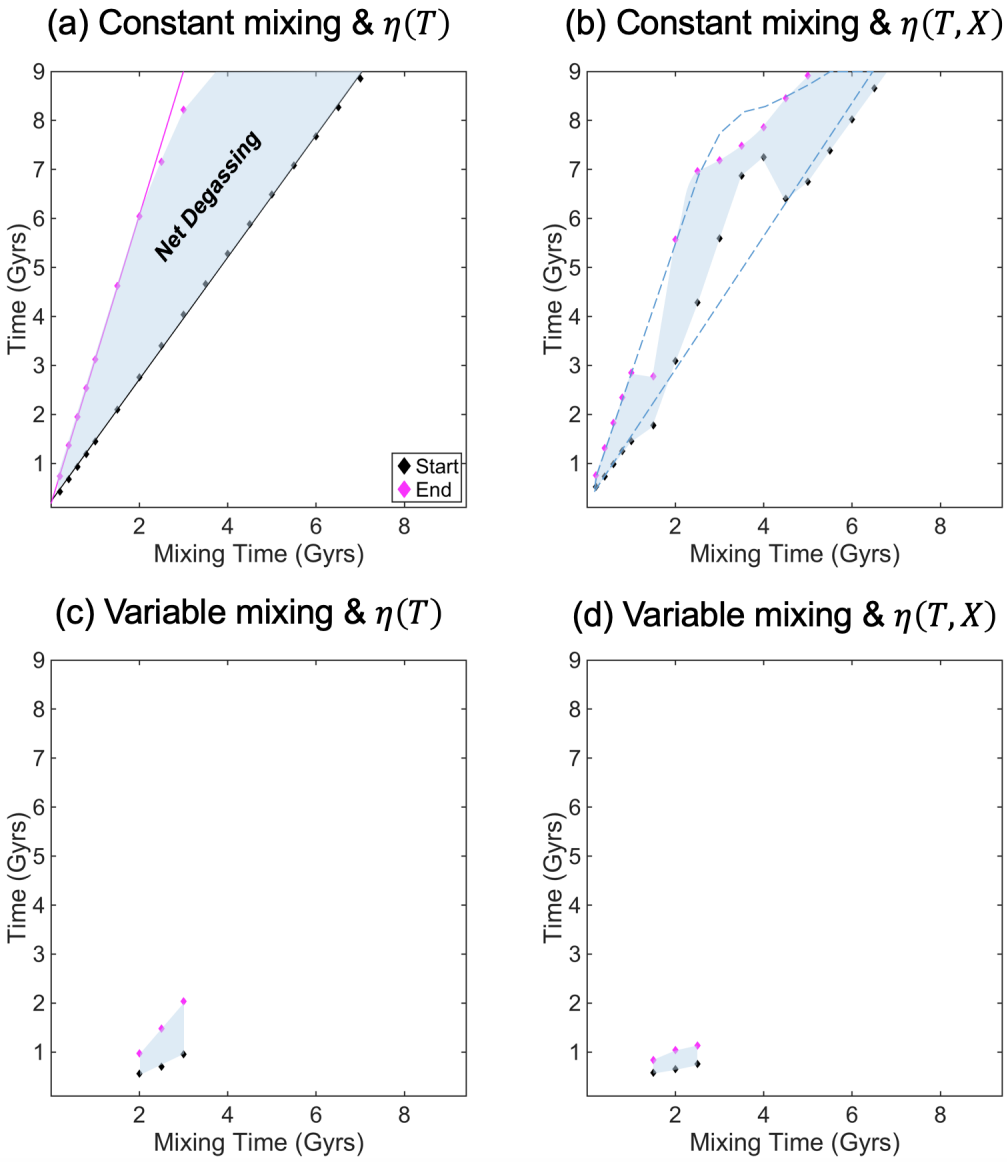

Figure 8: COLOUR The start (black diamonds) and end (magenta diamonds) of periods of net degassing for constant mixing, variable mixing, and both viscosity laws. Where there are no points, no net degassing period occurs. A linear trend is fitted to $\tau_{(Ra)} < 2$ Gyrs. The y-axis corresponds to the x-axis in Figures 4 to 7. Shaded regions corresponds to net degassing . The water-dependent viscosity shortens the period of degassing whilst variable mixing severely restricts the occurrence of degassing.

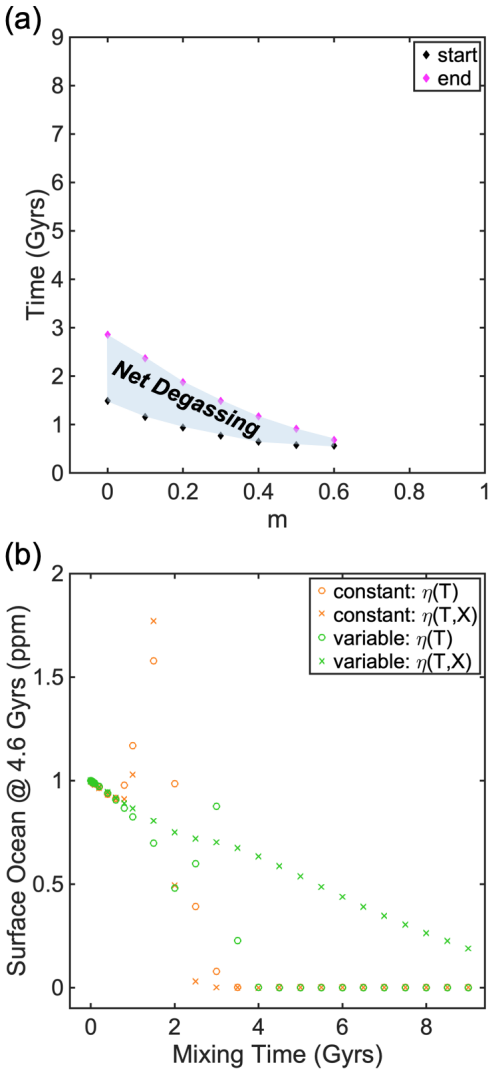

Figure 9: COLOUR (a) Net degassing region for variations in m, akin to Figure 8 and (b) number of surface oceans at 4.6 Gyrs in each of the models in Figure 8, normalised by Earth's present day ocean volume (1.39×10^{21} kg).

Appendix

Parameters	Symbol	Value				Units
present day time	t_{pd}	4.6				Gyrs
thermal expansion	α	2.5×10^{-5}				K^{-1}
density	ρ	3500				kgm^{-3}
gravity	g	10				ms^{-2}
mantle depth	d	2.88×10^{6}				m
mantle volume	V	9.05×10^{20}				m^3
surface area*	S	71%				-
average plate length	L	$2d$				m
thermal diffusivity	κ	8.57×10^{-7}				m^2
specific heat capacity	c_p	1000				$Jkg^{-1}K^{-1}$
thermal conductivity	k_c	3				$Wm^{-1}K^{-1}$
degassing efficiency	F_d	1				-
regassing efficiency	F_r	0.15				-
plate water content	X_p	2600				ppm
	z_1	286				mK^{-1}
melting depth constants**	z_2	164				$mppm^{-1}$
	z_3	-3.266×10^{5}				m
elements	j	U^{238}	U^{235}	Th	K	-
concentration	C_j	30.8	0.22	124	36.9	10^{-9} $kgkg^{-1}$
heat production	H_j	9.46	56.9	2.64	2.92	10^{-5} Wkg^{-1}
half-life	τ_j	4.47	0.704	14	1.25	Gyrs

Table 2: Table of constant parameters. *oceanic basin surface area of Earth, **(Hirschmann et al., 2009; Crowley et al., 2011).

		H_{sf}
Mixing Time (Gyrs)	0.6	1.614
	0.8	1.599
	1	1.687
	1.5	2.541
	20	1.510
	2.5	1.405
	3	1.345
	3.5	1.311
	4	1.357
	4.5	1.623
	5-10	1.722
m	0	1.687
	0.1	1.611
	0.2	1.599
	0.3	1.616

Table 3: Table of H_{sf} values to constrain to 46 TW for $\eta(T, X)$ constant mixing and $\eta(T, X)$ variable mixing for different values of m.